Modeling and optimizing irradiance on planar, folded, and honeycomb shapes to maximize photocatalytic air purification

Jérôme Taranto [a,b,1], Didier Frochot [a,*], Pierre Pichat [b,**]

[a] *EDF-Les Renardières, 77818 Moret-sur-Loing, France*
[b] *Photocatalyse et Environnement, CNRS UMR "IFoS", STMS, Ecole Centrale de Lyon, 69134 Ecully Cedex, France*

Abstract

Photocatalytic purification of indoor air requires devices that are compact and ensure good contact between the air flow and the photocatalyst-coated material with a minimal pressure drop. These three conditions lead to materials-destined to be coated by a photocatalyst-having complex shapes. Accordingly, modeling becomes essential in optimizing the irradiance of the photocatalytic support, which obviously is a factor of paramount importance. We present here a methodical strategy to optimize irradiance on a regularly folded and a honeycomb-shaped material. The first step was to calculate the irradiance on a planar material. The surface of the UV lamp tubes was modeled as an ensemble of elemental lighting sources emitting according to a Lambert law. After the validity was verified by irradiance measurements, similar calculations were performed for a folded and a honeycomb-shaped material, using appropriate geometrical parameters. Using an experimental design (Doehlert matrix), the effects of the interval between the lamps, the distance between the lamps and the material, and the geometrical characteristics of the folds or the honeycomb cells upon the homogeneity and value of the irradiance were calculated. Finally, a multicriterion analysis was employed to determine the configuration producing optimal irradiance. The methodology can easily be applied to UV lamps and reactors having dimensions different from those used in our calculations.

1. Introduction

Air purifiers need to be as compact as possible, whatever the technology they are based upon. This requirement is crucial for indoor air, whether the purifier is designed for individual rooms or entire buildings. Small dimensions are also sought when treating gaseous effluents of various kinds. In particular, photocatalytic purifiers generally consist of alternate banks of UV lamps and TiO_2-coated materials through which the air to be purified is flowed [1–6] as shown in Fig. 1. Therefore, compactness means increasing the ratio of the photocatalytic material geometrical area to the purifier volume, which in general leads to complex shapes of the material. Also, good contact between the air and the photocatalyst is necessary, while the pressure drop must remain low as in any type of air purifier; this leads to the use of porous or multichannel materials. Consequently, determining the optimum configuration of lamps and the material in the purifier to obtain an irradiance of this material as high and homogeneous as possible becomes extremely difficult. Measurements of irradiance at the material surface are most often impossible. Measurements of the photocatalytic efficacy for several configurations are time-consuming; the results cannot even be reliably used to find the optimum irradiance as the efficacy ranking depends on conditions other than the irradiance, such as, *inter alia*, the nature and partial pressure of the pollutant used in the photocatalytic tests.

Therefore, we think that experimental design is the best method for determining optimum irradiance when materials of complex shapes are employed. The experimental design methodology was used for planning the experimentation and for analyzing the experimental results. In this methodology, the levels (or settings or values) of the independent variables are

* Corresponding author.
** Corresponding author. Tel. +33 4 78 660550; fax: +33 4 78 331140.
  E-mail addresses: tarantoj@ecpm.u-strasbg.fr (J. Taranto),
didier.frochot@edf.fr (D. Frochot), pichat@ec-lyon.fr (P. Pichat).
  [1] Present address: Laboratoire des Matériaux, Surfaces et Procédés pour la Catalyse, CNRS UMR 7515, 25 rue Becquerel, 67087 Strasbourg Cedex 2, France.
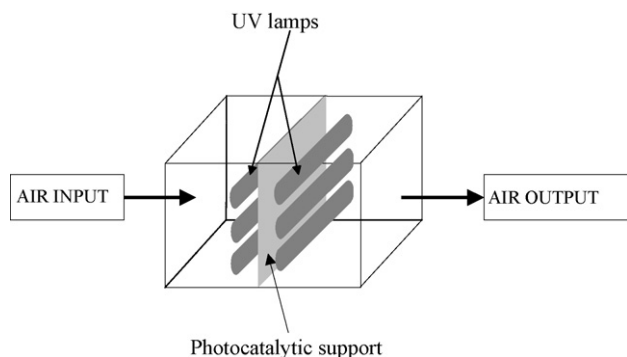
Fig. 1. Scheme of a common photocatalytic air cleaner.

Fig. 2. U-shaped lamps dimensions ($C = 225$ mm, $D = 37$ mm, and $D_1 = 17$ mm).

simultaneously modified from one computer experiment to another. This provides the means of obtaining a statistically significant model of a phenomenon by performing a minimum set of experiments adequately distributed in the experimental region (experimental matrix). A large number of experimental designs adapted to various types of problems are available, such as factorial designs, centroid composite matrices and Doehlert matrix [7,8]. Moreover, they allow finding possible interactions between parameters.

In this study, we have developed a computational program, and we have first applied it to the simple case of irradiance distribution on a planar material in order to check the calculated irradiance against the measured irradiance. The model established for the planar material was then appropriately modified for a folded material and a honeycomb-shaped material. A Doehlert matrix [7] was used to determine the configuration for optimal irradiance for the folded and honeycomb-shaped materials by taking into consideration geometrical factors related to these shapes. Our calculations and the limits on the parameters take into account a given reactor and lamps of a particular type (see Section 2) which we used in photocatalytic experiments whose results will be published elsewhere. However, the methodology described here can easily be applied to reactors and lamps having other dimensions. The objective was to model the irradiance distribution on the material (destined to be coated by various types of photocatalysts) for the rays emitted by the lamps and reaching the material directly, thus eliminating effects of the wavelength or the reflection and dispersion of light by the material (whose optical properties can vary substantially) which were taken into account in previous modeling regarding honeycomb monoliths [1–5] and parallel planar meshes [9]. In fact, the incident photons are the most important factor since the fraction of these photons absorbed by the photocatalyst is expected to be large (*e.g.*, ~92% according to Ref. [10]) with respect to reflection and scattering.

2. Experimental

To validate our calculations concerning a photocatalytic planar material and to fix limits to the parameters of our modeling whatever the shape of the material, we used a parallelepiped (56 cm × 29.5 cm × 20 cm) where the UV lamps and the photocatalytic materials can be accommodated (Fig. 1). This
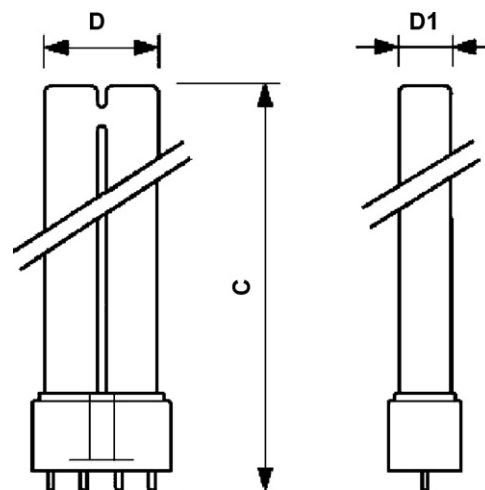
parallelepiped is part of a close loop reactor we employed for photocatalytic experiments as will be reported in another paper.

The PL-L TUV Philips lamps used in our modeling and measurements of irradiance comprise two tubes and have the dimensions indicated in Fig. 2. Their electrical power is either 18 or 35 W. Two peculiarities have been taken into account in this study: (i) although the quartz part of each tube is *ca.* 192 mm in length, the actual emitting length was evaluated to be only 170 mm because of ''dead zones'' at the extremities and (ii) as the diameter of the tubes is great with respect to the space between the two tubes, shading effects of one tube over the other occur. Note that, as mentioned in Section 1, our calculations of irradiance do not depend on the wavelength.

Irradiance on the planar photocatalytic material was measured with an International Light IL1700 radiometer and an IL1771 sensor specially designed for lighting sources emitting at 254 nm, which is the case of the PL-L TUV Philips lamps.

3. Modeling irradiance on a planar material

As aforementioned, compactness of photocatalytic air purifiers is highly desirable. Consequently, the distance between the lamps and the photocatalytic materials is usually too small for assimilating the UV tubes to point sources. The external surface of the cylindrical lamp is considered to consist of N identical elemental sources S separated from one another by a distance dl. This surface is assumed to irradiate according to the Lambert law. The purpose of the calculation is to express the irradiation at a point M of the material as a function of geometrical parameters and of the radiance L of S (L is the radiant power per area and per solid angle unit). The geometrical parameters are the lamp radius r, the distance d_M between M and S and three angles defining, together with d_M, both the position of M with respect to the lamp and the fraction of the lamp surface that irradiates M. These angles are: α_M, the angle between the perpendicular to the irradiated material and segment MS, θ_M, the angle between segment MS and the perpendicular to the lamp axis passing through S, and
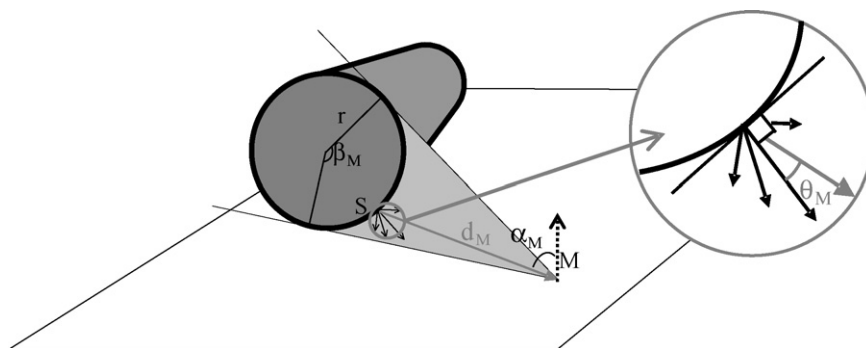
Fig. 3. Irradiance from a point S of the UV tube to a point M of the plane material.

β_M, the angle related to the arc from which M is irradiated (Fig. 3). θ_M takes into account the fact that only one of the rays emitted by each S reaches M. β_M allows for the screening effect of one tube on the other. Considering in a first stage that S are point sources (viz. sources emitting in all space directions), the basic relationship giving the irradiance E_M at M from S is:
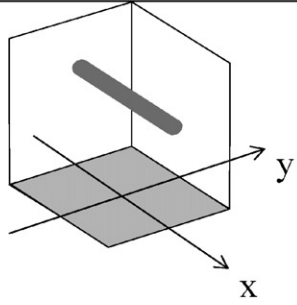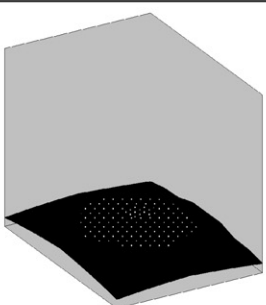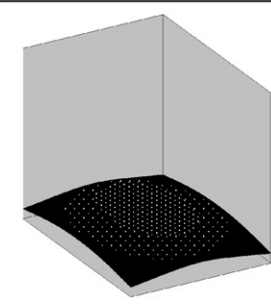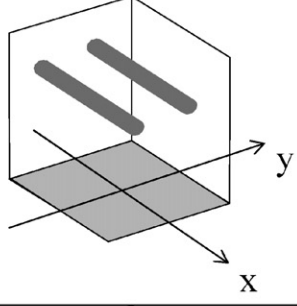
$$E_M = \frac{I \times \cos \alpha_M}{d_M^2}$$

(1)
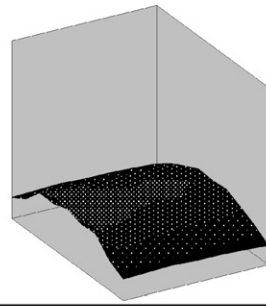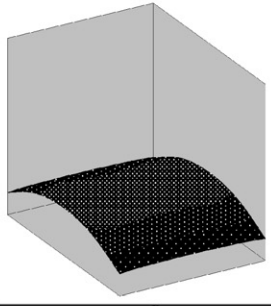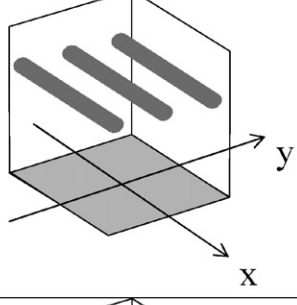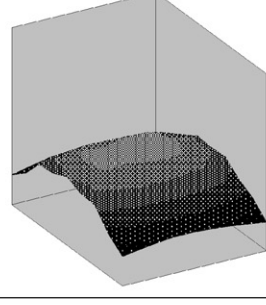
Table 1
(a) Distribution of measured and calculated irradiance in function of distance d between the lamps and the planar material, (b) of the number of lamps irradiating a planar material and (c) of electrical power of the lamp

Distance (mm)		Distribution of measured irradiance	Distribution of calculated irradiance
25			
77			
225			

(a)

Table 1 (*Continued*)

Number of lamps		Distribution of measured irradiance	Distribution of calculated irradiance
1			
2			
3			
4			

(b)

where I is the radiant power of S. For N point sources, it becomes:
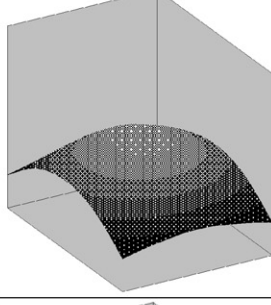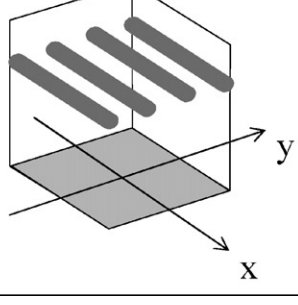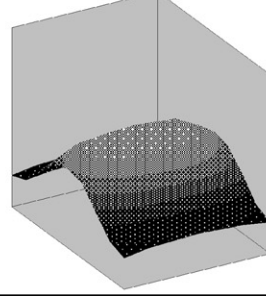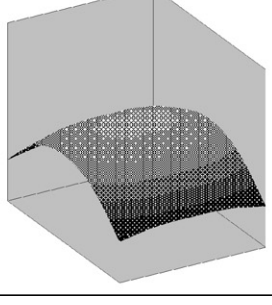
$$E_M = \frac{1}{N_M} \times \int_{i=1}^{i=N_M} \frac{dI_{i,M} \times \cos \alpha_{i,M}}{d_{i,M}^2}. \tag{2}$$

Taking account of θ_M, and considering that the irradiating surface of the lamp can be divided into rectangular elements whose surface area is equal to $2r \sin(\beta_M/2) \times dl$ (the infinitesimal surface area in the direction perpendicular to the cylindrical lamp axis) and that each S irradiates
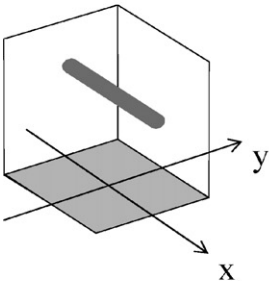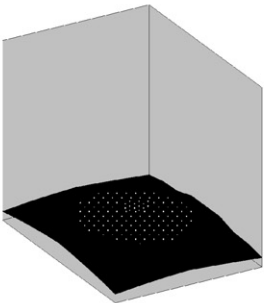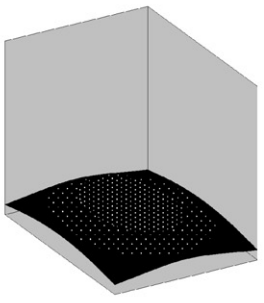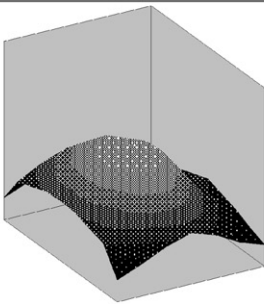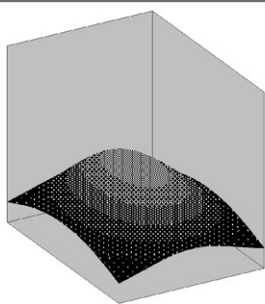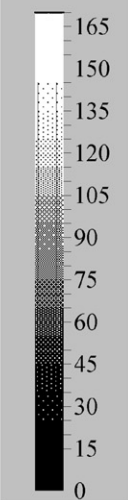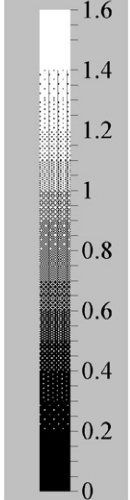
according to the Lambert law, $dI_{i,M}$ for the ith S is related to L by:

$$dI_{i,M} = L \times 2r \sin\left(\frac{\beta_M}{2}\right) \times dl \times \cos \theta_{i,M}. \tag{3}$$

Combining Eqs. (2) and (3), the resulting irradiance of M by the N elemental sources S is:

$$E_M = \frac{L \times 2r \sin(\beta_M/2)}{N_M} \times \int_{i=1}^{i=N_M} \frac{\cos \theta_{i,M} \times \cos \alpha_{i,M}}{d_{i,M}^2} \times dl \tag{4}$$

Table 1 (*Continued*)

Lamp electrical power (W)		Distribution of measured irradiance	Distribution of calculated irradiance
18			
35			
scale		W m^{-2}	no dimension

(c)

This relationship allows one to calculate the irradiance distribution on the planar material. For that, we used the Excel spreadsheet.

The agreement between the calculated and experimental irradiance values was satisfactory in all conditions (Table 1). It was further improved when the specular reflection on the stainless steel bottom wall of the parallelepiped constituting the photocatalytic reactor was considered (reflecting factor on stainless steel: 0.3 at 254 nm) as shown in Table 2. The parameters were the number of lamps (1–4) symmetrically situated at prefixed intervals, the distance (25, 77 or 225 mm) between the irradiated material and the plane containing the axes of the lamps, and the electrical power of the lamps (18 or 35 W for the same dimensions). E was measured at 63 points of

the irradiated material (16.5 cm × 25.5 cm = 408 cm^2), these points being separated by 25 mm from one another.

In short, our calculation can be regarded as validated. That encouraged us to determine the irradiance distribution for complex shapes, *viz.* a regularly folded material and a honeycomb.

4. Modeling irradiance on a folded material

The previous calculation cannot be used for the sides of the folds as the corresponding planes are not parallel to the lamps axes as is the case for the planar material. However, since the objective is to find the configuration providing an irradiance E of the material as high and homogeneous as possible, it was

Table 2
Comparison between calculated irradiance (in taking or not into account light reflection onto the reactor wall) and measured irradiance on a planar material irradiated by two UV lamps
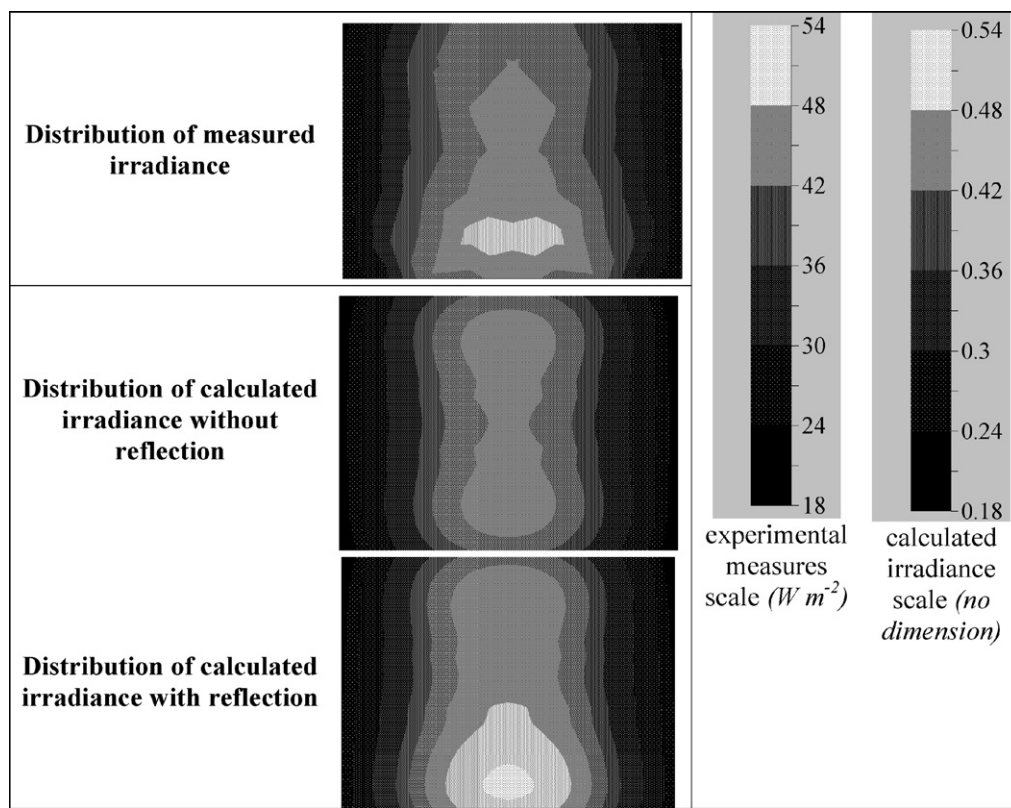
thought possible to achieve this goal by calculating the irradiance only at the top and bottom of the folds which are both situated in planes parallel to the lamps axes.

The folding was characterized by the angle of the folds and the length of the sides (Table 3). It obviously affects the distance between the plane containing the axes of the lamps and the plane passing through the middles of the folds of the irradiated material. Along with the space between the lamps, these variables are the four factors U_i affecting E (Table 3); the factors U_i are also called natural variables. In an experimental study, the higher the number of factors (*i.e.*, parameters controlled by the experimentalist), the more difficult the determination of an optimum, especially if these factors are not intrinsically independent. Varying the value (also called level) of only one factor while keeping the others constant is inappropriate for various reasons [11]. Allowing all the factors to vary at the same time by use of an experimental design is not a drawback but, on the contrary, presents many advantages: (i) a

decrease in the number of experiments, (ii) an increase in the number of factors, (iii) the detection of interactions between factors, (iv) finding optima, (v) a better precision of the results, and (vi) optimizing the results.

In these designs, the levels of the independent variables (natural variables U_i) are normalized, usually as reduced and centred variables X_i (normalized variables), for easier data treatment and analysis. Transformation of natural variables into normalized variables is made *via*. the following equation:

$$X_{ij} = \frac{U_{ij} - U_i^0}{\Delta U_i} \qquad (5)$$

where X_{ij} is the value of normalized variable X_i in experiment j, U_{ij} the value of natural variable U_i in experiment j, U_i^0 the value of natural variable U_i in the centre of the domain of interest (it corresponds to $X_i = 0$), and ΔU_i is the variation of the natural variable U_i corresponding to a variation of the normalized variable X_i equal to +1.

Given the dimensions of the parallelepiped reactor and of the lamps (*vide supra*), the borders of each X_i were those indicated in Table 3. No more than five lamps were considered in the model since a sixth had little effect on E as was shown by the measurements carried out for the planar material whose area was limited by the dimensions of the reactor. The following modeling was hence performed for up to five lamps irradiating one face of the folded material.

Table 3
Studied factors and experimental domain for the folded material

Factors	Level −1	Level +1
Distance lamps/folded material (mm), U_1	20	60
Space between lamps themselves (mm), U_2	50	100
Folds angle (°), U_3	30	90
Length of folds sides (mm), U_4	5	20

The experimental responses Y_1 and Y_2, chosen to quantify the homogeneity of the irradiance, were the irradiance standard deviation along the y-axis (*i.e.*, the axis perpendicular to the lamps axes; Table 1) for the points of the material located at the top and bottom of the folds (Y_1), and at the top only (Y_2). The irradiance standard deviation for the bottom was not taken into account as it could be deduced from Y_1 and Y_2, which are given by:

$$Y_1 = \sigma_{(y)} = \frac{1}{L} \sqrt{\left(\frac{\sum_{i=1}^{i=M} (E_{i(y)} - \bar{E}_{(y)})^2}{M - 1} \right)} \qquad (6)$$

$$Y_2 = \sigma_{(y,\text{tops})} = \frac{1}{L} \sqrt{\left(\frac{\sum_{i=1}^{i=M'} (E_{i(y,\text{tops})} - \bar{E}_{(y,\text{tops})})^2}{M' - 1} \right)} \qquad (7)$$

where M and M' are the number of y-axis points corresponding, respectively, to both the tops and bottoms of the folded material or to the tops only, E_i the irradiance value for point i, and $\bar{E}$ is the irradiance mean value. The third experimental response Y_3 is the maximum value of E divided by L (L being constant and not quantified) on the whole surface of the folded material:

$$Y_3 = \frac{E_{\max}}{L}. \qquad (8)$$

The choice of the Doehlert matrix [7] to model E is justified by several advantages of this matrix, among which: (i) the possibility of having a uniform distribution of experimental points in the domain studied, and of exploring the whole domain, (ii) the fact that the interactions between the factors are taken into account without increasing the number of "computer experiments" (*viz.* $k^2 + k + 1$, where k is the number of studied factors, that is, 4 in the present case and therefore 21 experiments), (iii) the possibility of using different numbers of levels for each X_i (3 for the first factor, 5 for the last one and 7 for the others), and (iv) the simultaneous optimization of several Y_i by use of a multicriterion analysis (denoted "desirability"), which allows one to adjust the weight of each Y_i (*e.g.*, a higher coefficient can be attributed to Y_1 and/or Y_2 if a homogeneous E is preferred to a high E).

The mathematical model chosen is a second-degree polynomial where first-order interactions between the X_i are taken into account:

$$\begin{aligned} Y_1 = {} & b_0 + b_1 X_1 + b_2 X_2 + b_3 X_3 + b_4 X_4 + b_{11} X_1 X_1 + b_{22} X_2 X_2 \\ & + b_{33} X_3 X_3 + b_{44} X_4 X_4 + b_{12} X_1 X_2 + b_{13} X_1 X_3 + b_{14} X_1 X_4 \\ & + b_{23} X_2 X_3 + b_{24} X_2 X_4 + b_{34} X_3 X_4 \end{aligned} \qquad (9)$$

where b_0 is the value at the centre of the experimental domain, b_i and b_{ii}, respectively, the first and the second order coefficients, and b_{ij} is the interaction effect between X_i and X_j factors. Equivalent expressions are written for Y_2 and Y_3 with different sets of coefficients. The 21 experiments obtained by means of the NemrodW$^{\copyright}$ software (LPRAI Company, France) have been modeled (for more details, see [6]), and the corresponding irradiance distributions graphically represented in three dimensions as shown in Table 4 for the two first experiments.

In addition, the NemrodW software indicates the most significant b_i coefficients. In statistics, the significance test is generally used to determine the acceptability of a value. In the present case, the hypothesis for the calculus of the significance is that all the coefficients b_i, b_{ii}, and b_{ij} are nil. The non-nil coefficients, as calculated by multilinear regression, were b_i and b_{11} for Y_1 and equivalents for Y_2 and Y_3. The dependency of E on the reciprocal of U_1^2 (U_1: distance lamps/folded material; (Eq. (1)) explains the fact that b_{11} is non-nil. Similarly, probabilities of 0.40, 4.03, and 0.36% for Y_1, Y_2, and Y_3, respectively, were obtained from the significance test of the multilinear regression; that means the regression was correct. Finally, the residues (*i.e.*, the difference between the experimental Y_i value and the Y_i value calculated using the polynomial model) must be independent of the Y_i value, randomly distributed with respect to the abscissa axis when plotted against the calculated Y_i, and aligned (Henry's line) when plotted against the probability (Fig. 4).

These prerequisites were verified for the three Y_i. Consequently, the polynomial was simplified to:

$$Y_1 = b_0 + b_1 X_1 + b_2 X_2 + b_3 X_3 + b_4 X_4 + b_{11} X_1 X_1 \qquad (10)$$

and equivalent polynomials for Y_2 and Y_3 with different sets of coefficients. Note that the significance of b_0 and equivalents was not considered as these coefficients do not influence Y_i through any X_i; they only indicate the Y_i value at the centre of the experimental domain.

New coefficients values were calculated using these simplified polynomials and their significance was also checked, along with the dispersion of the residues (Fig. 5). Only the values of b'_3 (for Y_2) and b''_3 (for Y_3) were found to be not significant. However, it does not necessarily mean that X_3 does not influence Y_2 and Y_3; the polynomial with interactions may not be suitable for X_3 in the experimental domain studied. X_3 must be varied since it influences Y_1. Therefore, b'_3 and b''_3 were also included, and the final polynomials were:

$$\begin{aligned} Y_1 = {} & 0.453 - 0.362 X_1 - 0.154 X_2 - 0.161 X_3 + 0.145 X_4 \\ & + 0.294 X_1 X_1 \end{aligned} \qquad (11)$$

$$\begin{aligned} Y_2 = {} & 0.113 - 0.343 X_1 + 0.114 X_2 + 0.030 X_3 + 0.112 X_4 \\ & + 0.366 X_1 X_1 \end{aligned} \qquad (12)$$
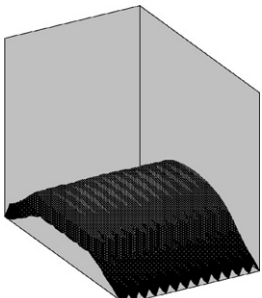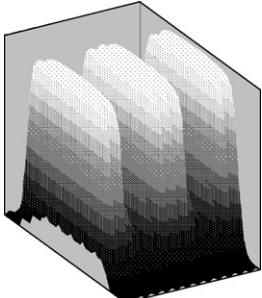
$$\begin{aligned} Y_3 = {} & 1.534 - 0.888 X_1 - 0.358 X_2 - 0.112 X_3 + 0.295 X_4 \\ & + 0.649 X_1 X_1 \end{aligned} \qquad (13)$$

These polynomials were employed to determine the values of each X_i for an E as homogeneous and high as possible. A multicriterion analysis allowed one to limit the study to the domain within which the desirability of each Y_i was between 0 and 100% (Fig. 6).

As expected, the desirability of Y_3 varied in an opposite way compared with the desirabilities of Y_1 and Y_2. In addition, a different weight can be attributed to the three responses: for example, a higher weight can be attributed to Y_1 and/or Y_2 if homogeneity is preferred to a high value of E (Y_3). In fact, even upon varying the relative weight attributed to the homogeneity

Table 4
Parameters, responses and irradiance distribution for two of the 21 experiments of the Doehlert matrix (folded material)

Exp.	Distance lamps-folded material (mm)	Space between lamps (mm)	Folds angle (°)	Length of the folds sides (mm)
(a) Experiments of the Doehlert matrix				
1	60.0	75.0	60.0	12.5
2	20.0	75.0	60.0	12.5

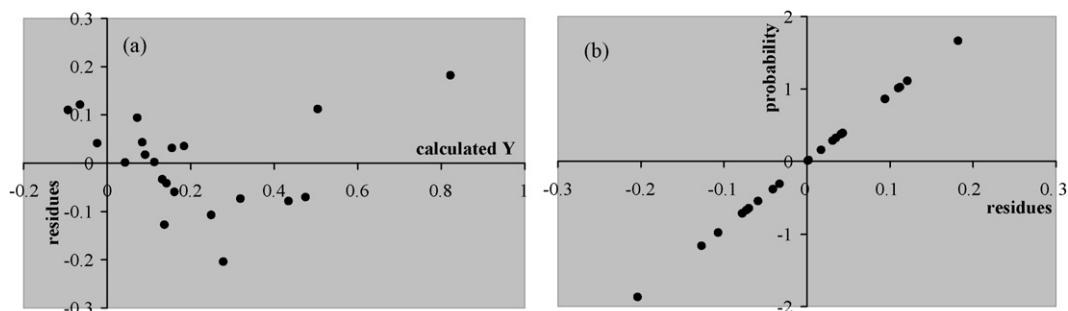| Exp.	Responses			Distribution of calculated irradiance
	$Y_1 = \sigma_{(y)}$	$Y_2 = \sigma_{(y,\text{folds})}$	$Y_3 = E_{\max}/L$	
(b) Responses and irradiance				
1	0.2938	0.0098	1.1026	
2	1.2221	1.0043	3.3287	

Fig. 4. (a) Residues distribution as a function of the calculated response and (b) normal plot of residues for polynomial (9).
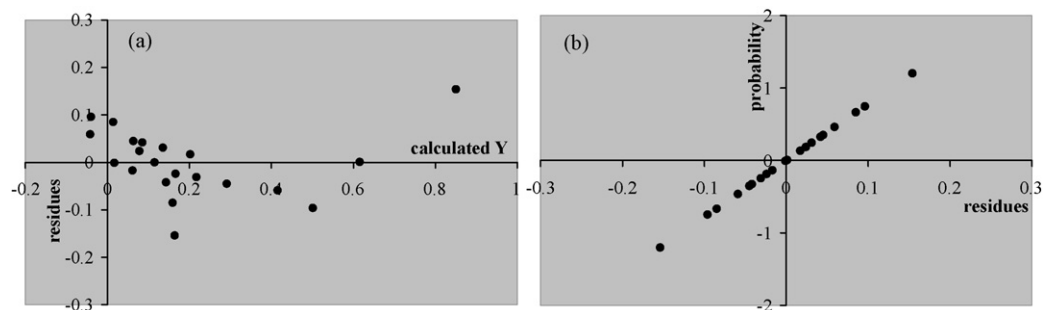

Fig. 5. (a) Residues distribution as a function of the calculated response and (b) normal plot of residues for polynomial (10).
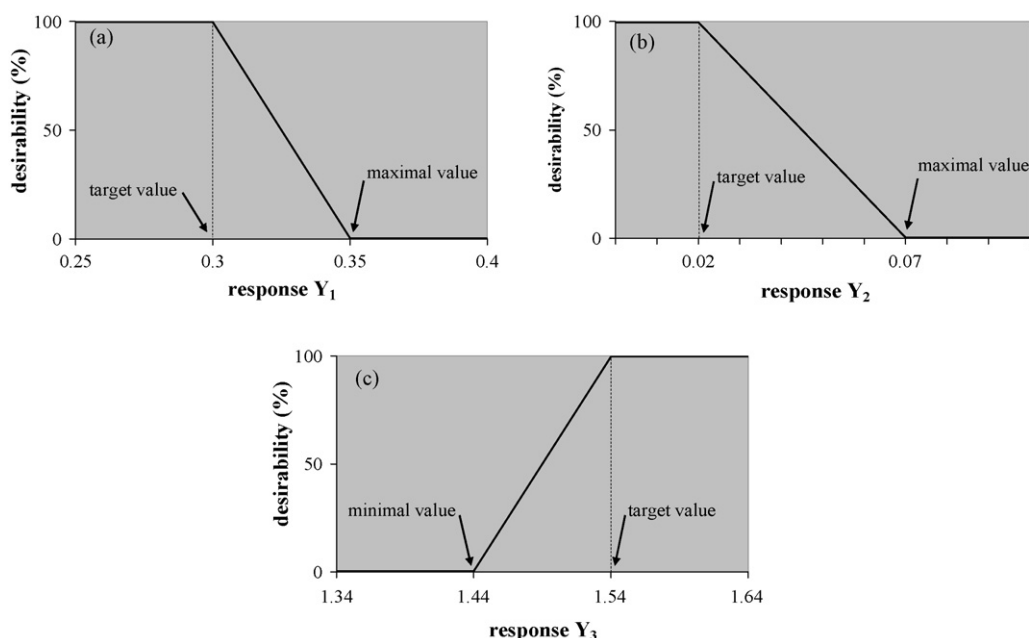
Fig. 6. Desirabilities of: (a) Y_1, (b) Y_2, and (c) Y_3.

Table 5
Configuration for optimum irradiance on a folded material

Variable	Value	Factor	Value
X_1	0.02	Distance lamps/fibrous material (mm)	40
X_2	−0.47	Space between lamps (mm)	62
X_3	0.86	Folds angle (°)	91
X_4	−0.22	Length of folds sides (mm)	10

by a factor of 10, Y_1 varied only between 0.32 and 0.35, Y_2 between 0.0244 and 0.0560, and Y_3 between 1.450 and 1.526. Finally, the best compromise derived from this polynomial model was obtained for the values indicated in Table 5 and the corresponding E distribution is shown in Fig. 7. Table 6 shows that the Y values calculated by the polynomials were close enough to those derived from the experimental design. Accordingly, the polynomials Eqs. (11)–(13) suffice to describe E. In practice, note that the optimum is achieved with the lamps relatively near the material (40 mm), a small length of the sides of the folds (10 mm), and an area of the folded material of 570 cm^2 corresponding to the same irradiated projected area, *viz.* 408 cm^2, as the non-folded material.

5. Modeling irradiance in a honeycomb material

The objective of the irradiance modeling in a honeycomb is the same as for the folded material, *i.e.*, to find the configuration providing an irradiance E of the material as high and homogeneous as possible. To carry out the calculation of E, the hexagonal honeycomb cells have been modeled as cylinders in line with what has been proposed previously for honeycomb cells with a square section [1,2,12]. Moreover, for simplification, only E at the centre M of the cell entrance face has been
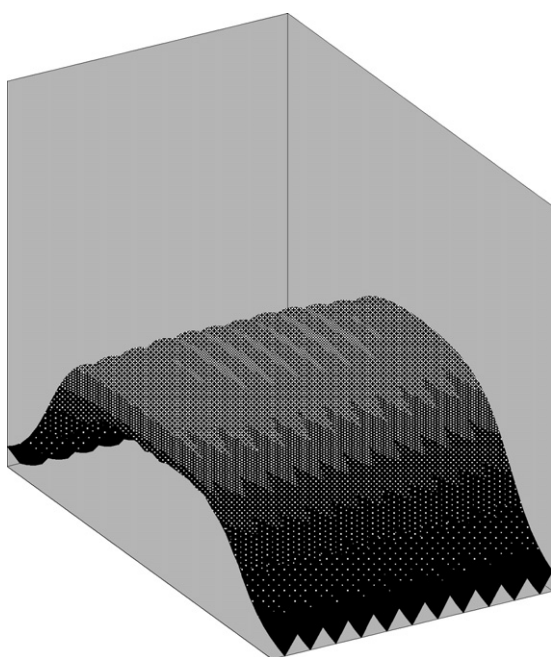
Fig. 7. Optimal irradiance distribution on a folded material.

Table 6
Comparison of the responses calculated by the computational modeling and by experimental design polynomials for the optimum configuration of the folded material

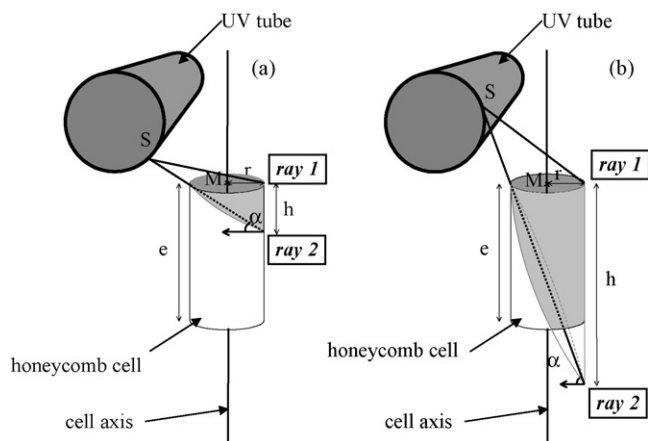| Responses	Computational modeling	Experimental design
Y_1, $\sigma_{(y)}$	0.3168	0.3204
Y_2, $\sigma_{(y,\text{tops})}$	0.0311	0.0229
Y_3, $E_{\max}/L$	1.6003	1.4531

Fig. 8. (a) No irradiation loss and (b) irradiation loss in a honeycomb cell.

calculated and considered as representing the average E for the cell entrance face. Contrary to the case of the calculations of E for the planar and the folded material, it is necessary here to take into account the area actually irradiated in the cell. For a light ray originating from S (S being a point of one of the two tubes of the U-shape lamp) and reaching the internal wall of a cylindrical cell with height h comprised between 0 and e (light beam limited by rays 1 and 2 in Fig. 8a), the irradiated area in cell i is given by:

$$dS_{irr,i,M} = \frac{1}{2} \times 2\pi r \times h_i \tag{14}$$

On replacing h_i by:

$$h_i = 2r \times \tan \alpha_i \tag{15}$$

it becomes:

$$dS_{irr,i,M} = 2\pi r^2 \times \tan \alpha_i \tag{16}$$

If h is greater than e (Fig. 8b), a part of the light beam from S limited by rays 1 and 2 does not contribute to the irradiation of the photocatalytic material. A more complex calculation shows that the irradiated area becomes:

$$dS_{irr,i,M} = r \times e \times \left[2\pi - \text{Arc}\cos\left(1 - \frac{e}{r \tan \alpha_i}\right) \right] \tag{17}$$

Note that for $e = h$, i.e., $\tan \alpha_i = e/2r$, Eqs. (16) and (17) give the same $\pi r e$ value for $dS_{irr,i,M}$. The expression of E is obtained from the value in Eq. (4) – calculated for a planar material – by multiplying this value by the ratio of the irradiated area, $dS_{irr,i,M}$, to the area, πr^2, of the planar entrance section of a cell (that is, the area that would be irradiated if the material were planar):

$$E_M = \frac{L \times 2r \sin(\beta_M/2)}{N_M \times \pi r^2} \times \int_{i=1}^{i=N_M} \frac{\cos \theta_{i,M} \times \cos \alpha_{i,M} \times dS_{irr,i,M}}{d_{i,M}^2}$$

$$\times \, dl \tag{18}$$

For the modeling, two of the factors X_i were obviously the same as in the case of the folded material, viz. the distance between the plane containing the axes of the lamps and the front face of the irradiated material, and the intervals between the five lamps. The borders of these factors (Table 7) were also the

Table 7
Factors influencing irradiance in a honeycomb material and borders of the study domain

Factors	Level −1	Level +1
Honeycomb length (mm), U_1	5	50
Distance lamps/honeycomb material (mm), U_2	20	60
Cell radius (mm), U_3	1.6	9.5
Space between lamps themselves (mm), U_4	50	100

same as they depend on the dimensions of the parallelepiped reactor (see Section 2). Two other factors represented the variations in E due to the honeycomb geometry: the radius of the cells modeled as cylinders and the honeycomb cell length. The limits of the cell radius depended on the honeycomb supplier. The honeycomb cell length, e, cannot be less than 5 mm because of the rigidity, and for $e > 50$ mm, E becomes very weak. The area of the honeycomb face was equal to that of the planar material, viz. 408 cm^2.

The experimental response Y_1 was used to evaluate the homogeneity of E as the standard deviation of the irradiance along the y-axis (i.e., the axis perpendicular to the lamps axes and parallel to the plane passing through the lamps axes) for each point M of one cell of the honeycomb located on this axis. Response Y_2 is the maximum value of E/L. As in the case of the folded material, a Doehlert matrix and second-degree polynomials with first-order interactions between X_i were utilized. The only difference was the ranking of the X_i common to the two cases (Tables 3 and 7). To limit the number of levels of the factor "honeycomb cell length" to 3 in order to simplify the calculations in the Excel spreadsheet, this factor was placed first; the distance between the lamps was ranked last so that its number of levels was 5. As previously, the 21 experiments obtained by means of the NemrodW software have been modeled, and the corresponding irradiance distributions graphically represented (for more details, see [6]). Table 8 shows two examples.

On proceeding as for the folded material, the polynomials can be simplified to:

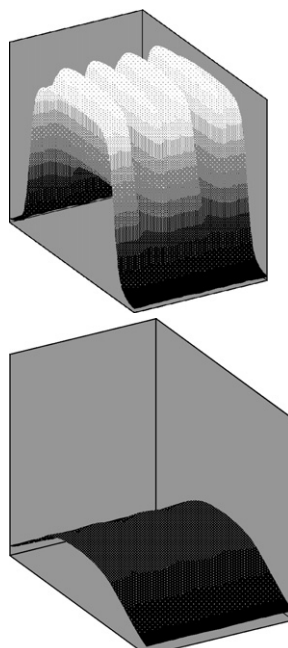$$Y_1 = b_0 + b_1 X_1 + b_2 X_2 + b_3 X_3 + b_4 X_4 + b_{22} X_2 X_2 + b_{44} X_4 X_4 + b_{12} X_1 X_2 \tag{19}$$

$$Y_2 = b_0' + b_1' X_1 + b_2' X_2 + b_3' X_3 + b_4' X_4 + b_{22}' X_2 X_2 + b_{44}' X_4 X_4 + b_{12}' X_1 X_2 \tag{20}$$

The significance tests showed that the factor "cell radius" (X_3) had a lower effect than the other X_i on Y_1 and Y_2 responses. Moreover, interaction between factors X_1 (honeycomb cell length) and X_2 (distance between the lamps axes and the honeycomb face) was important; it is linked to the distance of penetration of the light into the cells. Calculating new coefficients from these simplified polynomials, we obtained:

$$Y_1 = 0.129 + 0.109 X_1 - 0.427 X_2 - 0.028 X_3 + 0.057 X_4 + 0.526 X_2 X_2 + 0.209 X_4 X_4 - 0.331 X_1 X_2 \tag{21}$$

$$Y_2 = 2.834 + 0.799 X_1 - 1.740 X_2 - 0.067 X_3 - 1.244 X_4 + 1.289 X_2 X_2 + 0.991 X_4 X_4 - 0.848 X_1 X_2 \tag{22}$$

Table 8
Parameters, responses and irradiance distribution for two of the 21 experiments of the Doehlert matrix (honeycomb material)

Exp.	Honeycomb cell length (mm)	Distance lamps-honeycomb (mm)	Cell radius (mm)	Space between lamps (mm)
(a) Experiment of the Doehlert matrix				
5	38.75	20.00	5.55	75.00
18	16.25	46.67	6.54	100.00

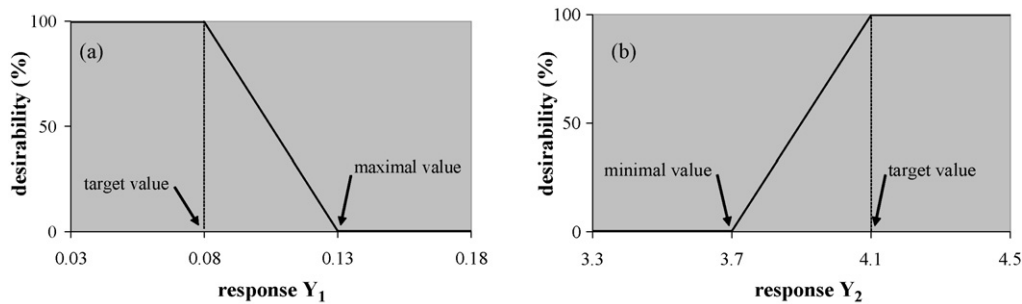| Exp.	Responses		Distribution of calculated irradiance
	$Y_1 = \sigma_{(y)}$	$Y_2 = E_{max}/L$	
(b) Responses and irradiance			
5	1.2467	6.3718	
18	0.0454	1.8057	

Fig. 9. Desirabilities of: (a) Y_1 and (b) Y_2.

In order to optimize E in the honeycomb material, target and maximum values were chosen to limit the desirability of each response (Fig. 9). As for the case of the folded material, the desirability of the response corresponding to the homogeneity or to the value of E varied in an opposite way. Similarly, results calculated by attributing different weights to the responses were relatively close. The best compromise was obtained for the values indicated in Table 9 and the corresponding E distribution is shown in Fig. 10. The ratio of the optimal honeycomb cell length (40 mm) to the optimal cell diameter (12.8 mm) was: 3.125. This ratio value is in excellent agreement with a previous model indicating that the flux on

the honeycomb walls falls to less than 1% of the incident flux for a ratio of 3 [4]. This means that in the case of the optimal honeycomb dimensions of Table 9, the incident flux is fully utilized.

Table 9
Configuration for optimum irradiance in a honeycomb material

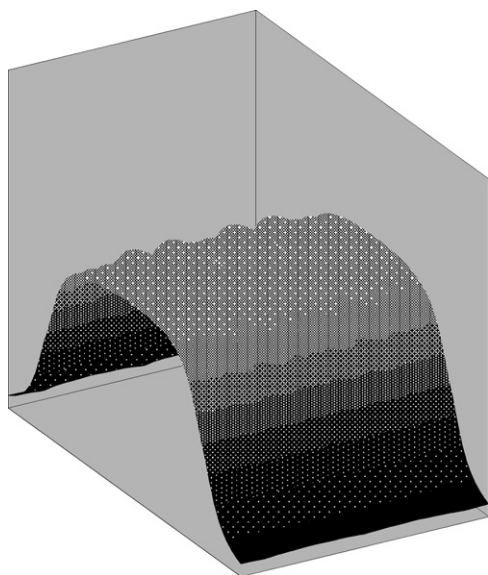| Variable	Value	Factor	Value
X_1	0.56	Honeycomb length (mm)	40
X_2	0.39	Distance lamps/honeycomb material (mm)	49
X_3	0.18	Cell radius (mm)	6.4
X_4	−0.73	Space between lamps themselves (mm)	52

Fig. 10. Optimal irradiance distribution in a honeycomb material.

Table 10
Comparison of the responses calculated by the computational modeling and by experimental design polynomials for the optimum configuration of the honeycomb material

Responses	Computational modeling	Experimental design
Y_1, $\sigma_{(y)}$	0.1341	0.1785
Y_2, E_{max}/L	3.9326	4.0289

Table 10 shows that the Y values calculated by the polynomials were close enough to those derived from the experimental design. Accordingly, the polynomials (Eqs. (21) and (22)) suffice to describe E.

The optimum distance between the axes of the lamps and the irradiated material (to the middle of the folds or cell entrance, respectively) and the optimum space between the lamps are significantly different for the honeycomb and the folded material (Tables 5 and 9) considering the dimensions of the reactor (see Section 2).

6. Conclusion

In this study, we have tackled the problem of the distribution of the irradiance E impinging on a material when both this material and the UV lamps have complex shapes as is most often the case in photocatalytic air purifiers. The examples treated correspond to commonly used U-shape lamps formed of two parallel cylindrical tubes (Fig. 2) irradiating either a folded material or a honeycomb-shaped material. The approach was to employ irradiance modeling combined with a Doehlert matrix to determine the best compromise between four interacting factors in order to achieve an E as high and homogeneously distributed as possible. These factors were the distance between the lamps and the material, the interval between the lamps, and two factors related to the geometry of the material. Limits to these factors were fixed by, *inter alia*, the dimensions of the

lamps (Fig. 2) and of the reactor (see Section 2) we used for photocatalytic experiments which will be reported elsewhere; but limits different from ours can readily be included in the calculations. The external surface of the lamp was assumed to irradiate according to the Lambert law and considered to consist of N identical elemental sources. This methodology was initially applied to the case of a planar material in order to be able to check its validity by measurements of E. The basic idea was then to consider that the calculation of E/L (L being the lamps' radiance) for the aforementioned complex shapes of the material can be derived from the calculation of E/L – using the methodology thus validated – on planes parallel to the axes of the lamps and passing through either the top or the bottom of the folds, or the entrances of the honeycomb cells. In this latter case, the calculation of the irradiated area in the cells was taken into account. A good agreement was found between E/L calculated by second-degree polynomials and by computational models; this indicates that a methodical experimental design, along with optical models, permit one to optimize E rapidly and with a satisfactory accuracy. Furthermore, it must be emphasized that these calculations can be performed by use of relatively simple means, for example, an Excel spreadsheet and any experimental design software.

Acknowledgement

References

[1] G.B. Raupp, Md.M. Hossain, Radiation field modeling in a photocatalytic monolith reactor, Chem. Eng. Sci. 53 (1998) 3771–3780.

[2] R.J. Hall, P. Bendfeldt, T.N. Obee, J.J. Sangiovanni, Computational and experimental studies of UV/titania photocatalytic oxidation of VOCs in honeycomb monoliths, J. Adv. Oxid. Technol. 3 (1998) 243–252.

[3] G.B. Raupp, Md.M. Hossain, Polychromatic radiation field model for a honeycomb monolith photocatalytic reactor, Chem. Eng. Sci. 54 (1999) 3027–3034.

[4] Md.M. Hossain, G.B. Raupp, S.O. Hay, T.N. Obee, Three-dimensional developing flow model for photocatalytic monolith reactors, AIChE J. 45 (1999) 1309–1321.

[5] G.B. Raupp, A. Alexiadis, Md.M. Hossain, R. Changrani, First-principles modelling, scaling laws and design of structured photocatalytic oxidation reactors for air purification, Catal. Today 69 (2001) 41–49.

[6] J. Taranto, Etude des effets de paramètres influençant l'efficacité d'un épurateur photocatalytique d'air, Modélisation et optimisation de l'éclairement sur des matériaux photocatalytiques plans, plissés et en nid d'abeilles, PhD Dissertation, Ecole Centrale de Lyon, Ecully, France, 2005.

[7] D.H. Doehlert, Uniform shell design, Appl. Stat. 19 (3) (1970) 231–239.

[8] A.I. Khuri, J.A. Cornell, Response Surfaces, Designs and Analyses, Marcel Dekker, ASQC Quality Press, New York, 1987.

[9] A.E. Cassano, C.R. Esterkin, A.C. Negro, O.M. Alfano, Radiation field inside a reactor of glass-fiber meshes coated with TiO$_2$, AIChE J. 48 (2002) 832–845.

[10] G.E. Imoberdorf, H.A. Irazoqui, A.E. Cassano, O.M. Alfano, Modeling of a multiannular photocatalytic reactor for perchloroethylene degradation in air, AIChE J. 52 (2006) 1814–1823.

[11] J. Goupy, Introduction aux plans d'expériences, 2ème éd., Dunod, 2001.

[12] Y. Luo, Reactor analysis for heterogeneous photocatalytic air purification processes, PhD Dissertation, North Carolina State University, 1994.